

Physics at a muon collider

H. Alida F. Hardersen

(Dated: March 2, 2020)

In this project we are studying the $\mu^+\mu^- \rightarrow b\bar{b}$ process at a future muon collider. I will be using the Trace method to calculate the transition matrices to be used in the differential cross section, Python(NumPy, scipy) for numerical integration and matplotlib for plotting. I will also use CompHEP for verifying my results. All constants(masses, decay widths etc are found in the 2018 version of the Particle Physics Booklet [2].

I. TRANSITION AMPLITUDES

There are three lowest order Feynman diagrams contributing to this process,

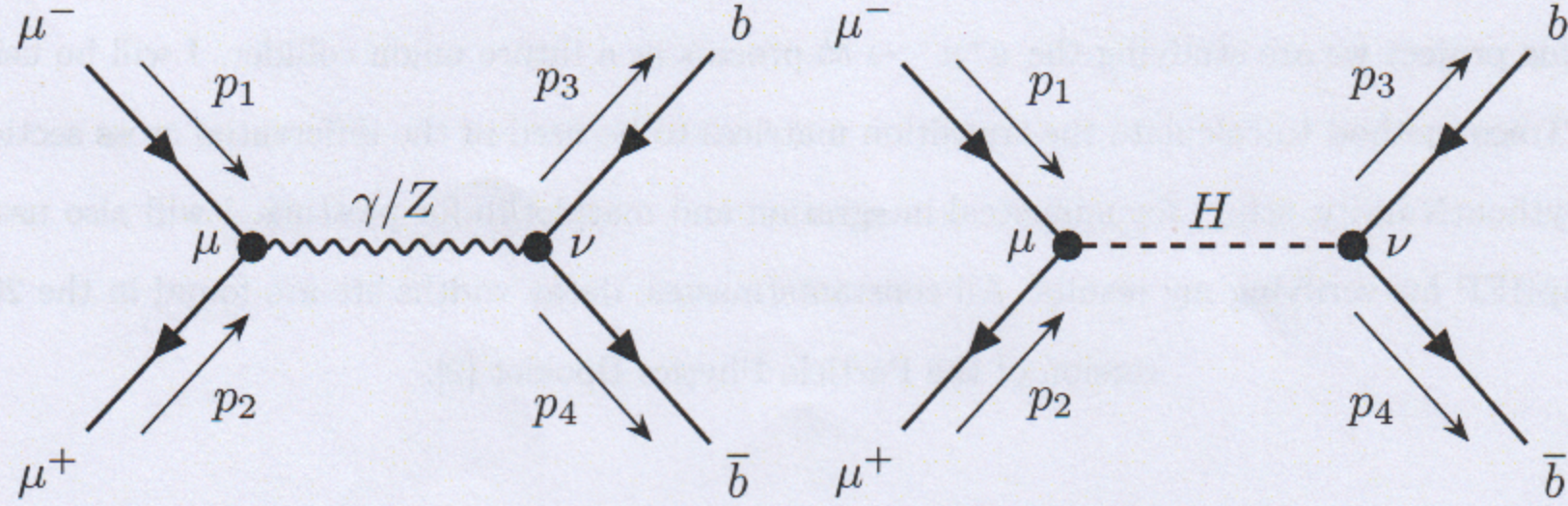


FIG. 1: Lowest order feynman diagrams contributing to the process

Using the Feynman rules [1] for the three diagrams we find the equations:

$$\begin{aligned} -i\mathcal{M}_\gamma &= [\bar{v}(p_2)ie\gamma^\mu u(p_1)] \frac{-ig_{\mu\nu}}{s} [\bar{u}(p_3)\frac{1}{3}ie\gamma^\nu v(p_4)] \\ -i\mathcal{M}_Z &= [\bar{v}(p_2)(-ig_z\gamma^\mu \frac{1}{2}(c_v^i - c_a^i\gamma^5))u(p_1)] \frac{-ig_{\mu\nu}}{s - m_Z^2} [\bar{u}(p_3)(-ig_z\gamma^\nu \frac{1}{2}(c_v^f - c_a^f\gamma^5))v(p_4)] \\ -i\mathcal{M}_H &= [\bar{v}(p_2)(-im_\mu \frac{g_w}{2m_w})u(p_1)] \frac{i}{s - m_H^2} [\bar{u}(p_3)(-im_b \frac{g_w}{2m_w})v(p_4)] \end{aligned}$$

The Z-and Higgs-bosons are unstable particles and this must be accounted for in the propagators using the particles total decay width $\Gamma_Z = 2.4952$ GeV and $\Gamma_H = 4.07$ MeV. Because $\Gamma_{Z,H} \ll m_{Z,H}$ we can make the following replacement in the propagator,

$$\frac{1}{s - m_{Z,H}^2} \rightarrow \frac{1}{s - m_{Z,H}^2 + im_{Z,H}\Gamma_{Z,H}} \quad (1)$$

which gives the three matrix elements:

$$\mathcal{M}_\gamma = -\frac{e^2}{3s} [\bar{v}(p_2)\gamma^\mu u(p_1)][\bar{u}(p_3)\gamma_\mu v(p_4)] \quad (2)$$

$$\mathcal{M}_Z = -\frac{g_z^2}{s - m_z^2 + im_z\Gamma_z} [\bar{v}(p_2)\gamma^\mu \frac{1}{2}(c_v^i - c_a^i\gamma^5)u(p_1)][\bar{u}(p_3)\gamma_\mu \frac{1}{2}(c_v^f - c_a^f\gamma^5)v(p_4)] \quad (3)$$

$$\mathcal{M}_H = \frac{g_w^2 m_\mu m_b}{4m_w^2(s - m_H^2 + im_H\Gamma_H)} [\bar{v}(p_2)u(p_1)][\bar{u}(p_3)v(p_4)] \quad (4)$$

II. DIFFERENTIAL CROSS-SECTION

The differential cross-section is given by

$$\frac{d\sigma}{d\Omega} = 3 \times \frac{1}{64\pi^2 s} \frac{|k|}{|p|} \langle |\mathcal{M}_{fi}|^2 \rangle \quad \text{with} \quad \langle |\mathcal{M}_{fi}|^2 \rangle = \langle |\mathcal{M}_\gamma + \mathcal{M}_Z + \mathcal{M}_H|^2 \rangle \quad (5)$$

Where the factor 3 accounts for the sum over the three possible colour configurations ($g\bar{g}$, $r\bar{r}$ and $b\bar{b}$) of the $b\bar{b}$ pair in the final state. We can then find the unpolarized differential cross-section by using $d\Omega = d(\cos\theta)d\phi$ and integrating over the azimuthal angle ϕ ,

$$\frac{d\sigma}{d\cos\theta} = \int_0^{2\pi} \frac{d\sigma}{d\Omega} d\phi = 2\pi \frac{d\sigma}{d\Omega} = 3 \times \frac{1}{32\pi s} \frac{|k|}{|p|} \langle |\mathcal{M}_{fi}|^2 \rangle \quad (6)$$

A. Matrix Elements

We must now determine the spin averaged transition amplitude squared $\langle |\mathcal{M}_{fi}|^2 \rangle$,

$$\begin{aligned} \langle |\mathcal{M}_{fi}|^2 \rangle &= \langle |\mathcal{M}_\gamma|^2 \rangle + \langle |\mathcal{M}_Z|^2 \rangle + \langle |\mathcal{M}_H|^2 \rangle \\ &+ \frac{1}{2} \left[\sum_{\text{spin}} \text{Re}\{\mathcal{M}_\gamma \mathcal{M}_Z^*\} + \sum_{\text{spin}} \text{Re}\{\mathcal{M}_\gamma \mathcal{M}_H^*\} + \sum_{\text{spin}} \text{Re}\{\mathcal{M}_Z \mathcal{M}_H^*\} \right] \end{aligned} \quad (7)$$

Each of the terms are found using the matrix elements (EQ. 2, 3, 4) and the trace formalism. I will name the interference terms \mathcal{X}_{ij} where $i, j = \gamma, H, Z$. The full calculations can be found in the Appendix. The diagram including the higgs boson will only give a very small contribution so the interference terms including \mathcal{M}_H can be neglected. We are therefore only left with the interference term between the Z and γ diagrams $\mathcal{X}_{\gamma Z}$, and the transition amplitudes,

$$\langle |\mathcal{M}_\gamma|^2 \rangle = \kappa_1 \left[(p_1 \cdot p_4)(p_2 \cdot p_3) + (p_1 \cdot p_3)(p_2 \cdot p_4) + m_b^2(p_1 \cdot p_2) + m_\mu^2(p_3 \cdot p_4) + 2m_\mu^2 m_b^2 \right] \quad (8)$$

$$\langle |\mathcal{M}_Z|^2 \rangle = \kappa_2 \left[(p_1 \cdot p_4)(p_2 \cdot p_3)f_1 + (p_1 \cdot p_3)(p_2 \cdot p_4)f_2 + m_b^2(p_1 \cdot p_2)f_3 + m_\mu^2(p_3 \cdot p_4)f_4 + 2m_\mu^2 m_b^2 f_5 \right] \quad (9)$$

$$\langle |\mathcal{M}_H|^2 \rangle = \kappa_3 \left[(p_1 \cdot p_2)(p_3 \cdot p_4) - m_b^2(p_1 \cdot p_2) - m_\mu^2(p_3 \cdot p_4) + m_\mu^2 m_b^2 \right] \quad (10)$$

$$\mathcal{X}_{\gamma Z} = \kappa_4 \left[(p_1 \cdot p_4)(p_2 \cdot p_3)g_1 + (p_1 \cdot p_3)(p_2 \cdot p_4)g_2 + g_3 \left[m_b^2(p_1 \cdot p_2) + m_\mu^2(p_3 \cdot p_4) + 2m_\mu^2 m_b^2 \right] \right] \quad (11)$$

where the constants κ_i and the vector-axial vector terms f_i and g_i are defined as,

$$\kappa_1 = \frac{8e^4}{9s^2}, \quad \kappa_2 = \frac{g_Z^4}{2[(s - m_Z^2)^2 + m_Z^2 \Gamma_Z^2]}, \quad \kappa_3 = \frac{g_w^4 m_\mu^2 m_b^2}{4m_w^4 [(s - m_H^2)^2 + m_H^2 \Gamma_H^2]}, \quad \kappa_4 = \frac{4e^2 g_Z^2}{3s(s - m_Z^2 - im_Z \Gamma_Z)}$$

and

$$\begin{aligned} f_1 &= (C_V^2 + C_A^2)(C_V^{b^2} + C_A^{b^2}) + C_V C_A C_V^b C_A^b, & f_2 &= (C_V^2 + C_A^2)(C_V^{b^2} + C_A^{b^2}) - C_V C_A C_V^b C_A^b \\ f_3 &= (C_V^2 + C_A^2)(C_V^{b^2} - C_A^{b^2}), & f_4 &= (C_V^2 - C_A^2)(C_V^{b^2} + C_A^{b^2}), & f_5 &= (C_V^2 - C_A^2)(C_V^{b^2} - C_A^{b^2}) \\ g_1 &= C_V C_V^b + C_A C_A^b, & g_2 &= C_V C_V^b - C_A C_A^b, & g_3 &= C_V C_V^b \end{aligned}$$

The values of the coupling constants used can be found in TAB. I.

B. Kinematics

In the center of mass frame illustrated in FIG.13 with $s = (p_1 + p_2)^2 = (2E)^2 = E_{cm}^2$, and $p = \sqrt{E^2 - m_\mu^2}$ and $k = \sqrt{E^2 - m_b^2}$ the four-vectors of the particles can be taken to be

$$\begin{array}{lll} p_1 = (E, 0, 0, p) & & (p_1 \cdot p_2) = E^2 + p^2 \\ p_2 = (E, 0, 0, -p) & \rightarrow & (p_1 \cdot p_3) = (p_2 \cdot p_4) = E^2 - pk \cos \theta \\ p_3 = (E, k \sin \theta, 0, k \cos \theta) & & (p_1 \cdot p_4) = (p_2 \cdot p_3) = E^2 + pk \cos \theta \\ p_4 = (E, -k \sin \theta, 0, -k \cos \theta) & & (p_3 \cdot p_4) = E^2 + k^2 \end{array}$$

C. Unpolarized differential cross-section

The values above are inserted into EQ.6 and the differential cross-section for the various processes are shown in FIG.2. The differential cross-section for the Higgs- boson is a straight line at approximately 2.96×10^{-7} pb/rad so the contribution to the total cross-section is very small as expected.

All the separate contributions to the differential cross-section is compared with data from CompHEP[5] in 3 to compare the validity of my algorithm and calculations. The data from calculations correspond well to the data from CompHEP, with some small discrepancies in the Higgs-contribution to the differential cross-section(FIG. 3c). Because this difference is very small, and the Higgs contribution to the total differential cross-section is small, this will be ignored.

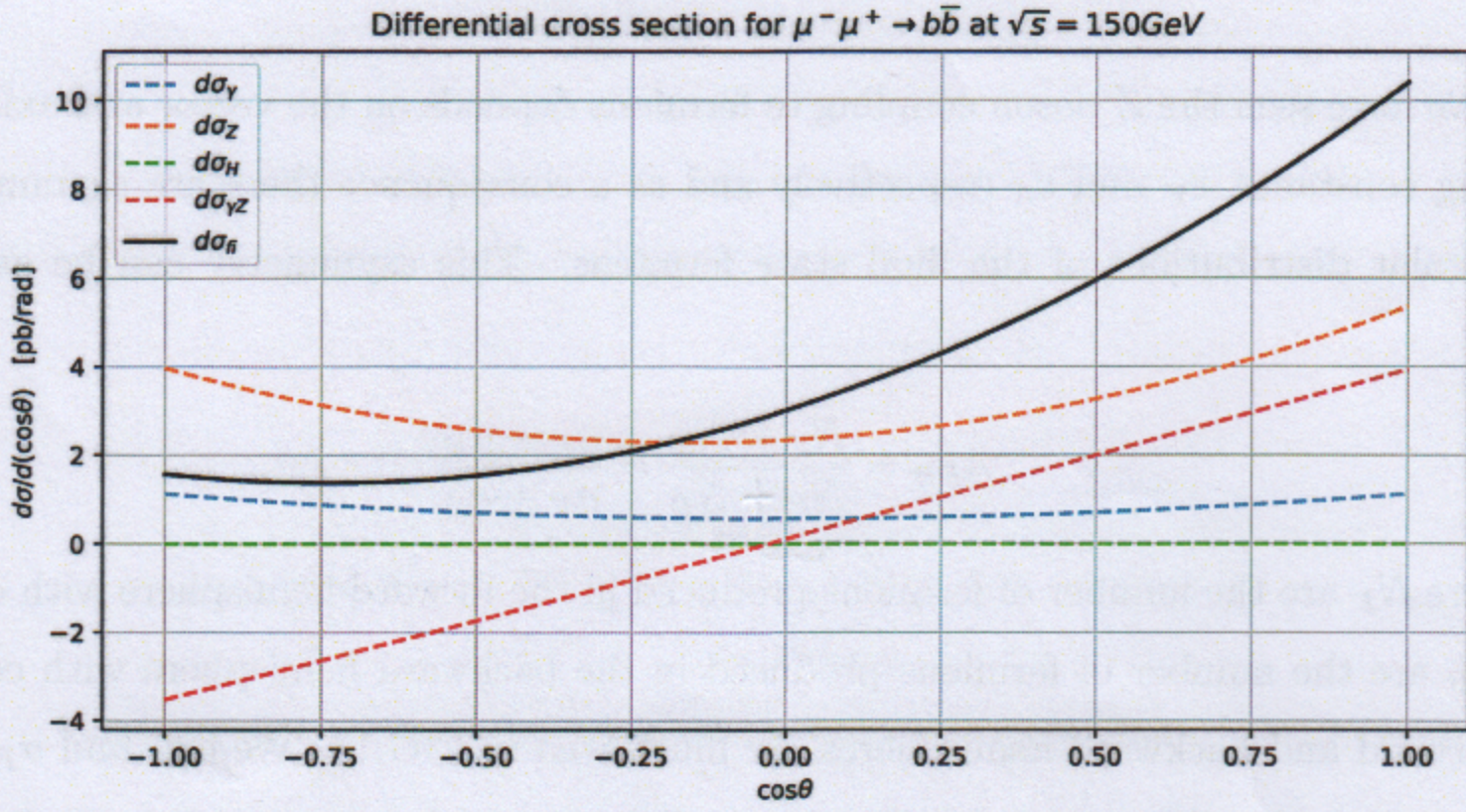


FIG. 2: All contributions to the differential cross-section compared with data generated in CompHEP. The colored lines are calculated using the trace method described above and the black plus(+) signs are generated using CompHEP.

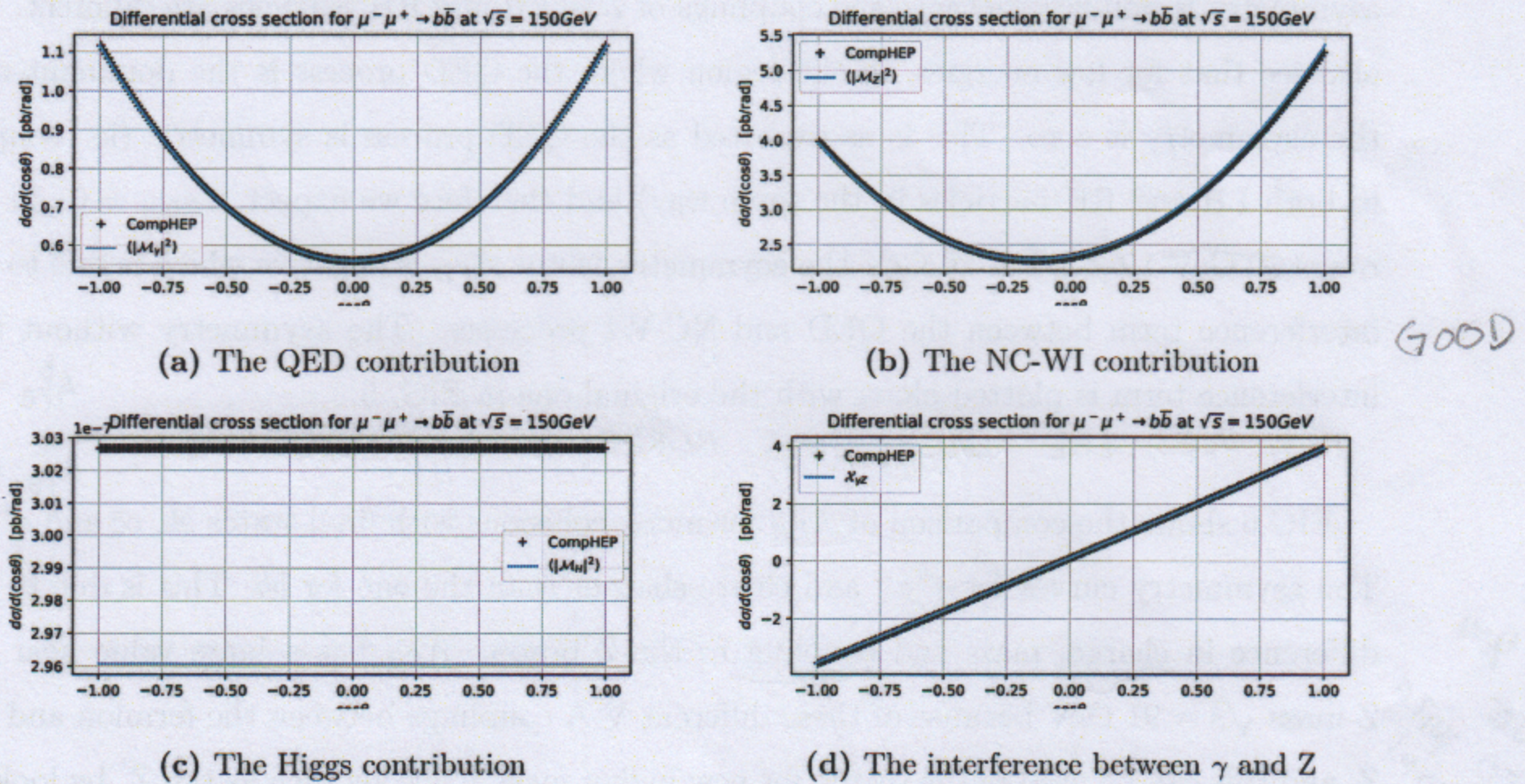


FIG. 3: Individual contributions to the differential cross-section. The black plus(+) sign represents data generated in CompHEP

III FORWARD-BACKWARD ASYMMETRY

III. FORWARD-BACKWARD ASYMMETRY

As we have seen the Z boson coupling to fermions depends on the vector and axial vector coupling constants, c_V and c_A respectively and as a consequence there are asymmetries in the angular distributions of the final state fermions. This asymmetry can be calculated using,

$$A_{FB} = \frac{N_F - N_B}{\underbrace{N_F + N_B}_{\sim}} = \frac{\sigma_F - \sigma_B}{\sigma_F + \sigma_B} \quad (12)$$

where N_F are the number of fermions produced in the forward hemisphere with $\cos \theta > 0$ and N_B are the number of fermions produced in the backward hemisphere with $\cos \theta < 0$. The forward and backward hemispheres are illustrated in FIG.13. We can find σ_F and σ_B by integrating the differential cross-section in EQ. 6 over the ranges $-1 < \cos \theta < 0$ and $0 < \cos \theta < 1$:

$$\sigma_F = \frac{N_f}{32\pi s} \frac{|k|}{|p|} \int_0^1 \langle |\mathcal{M}_{fi}|^2 \rangle d(\cos \theta) \quad \text{and} \quad \sigma_B = \frac{N_f}{32\pi s} \frac{|k|}{|p|} \int_{-1}^0 \langle |\mathcal{M}_{fi}|^2 \rangle d(\cos \theta) \quad (13)$$

We can see how A_{FB} depends on the center-of-mass energy \sqrt{s} in FIG. 12. The asymmetry is non-zero because the couplings of Z to LH and RH particles are different. We also see that for low energies, in the region where the QED process is the dominant one, the asymmetry is zero. This is as expected as the QED process is symmetric (ie. couples to both LH and RH particles in the same way) and therefore we expect $A_{FB,\gamma} = 0$. In the range $10 \text{ GeV} < \sqrt{s} < 86 \text{ GeV}$ the asymmetry factor A_{FB} is negative which is due to the interference term between the QED and NC-WI processes. The asymmetry without this interference term is plotted along with the original one in FIG. 5.

HOW DOES THE RED/BLUE CURVE AGREE WITH PREDICTION?

$$A_{FB}^b = \frac{3}{4} A_b A_p$$

$$A_{FB}^c = \frac{3}{4} A_c A_p$$

FIG.6 shows the comparison of A_{FB} for muon collisions with final states $b\bar{b}$, $c\bar{c}$ and e^+e^- . The asymmetry curves for e^+e^- and $c\bar{c}$ are sharper than the one for $b\bar{b}$. This is due to the difference in charge, mass and coupling to the Z boson. A_{FB} has a large value near the Z -mass $\sqrt{s} = 91 \text{ GeV}$ because of these different V-A couplings between the fermion and the Z , and this can be used in the search for new higher mass Z bosons such as the Z' by looking for a similar structure in the asymmetry.

$$A_{b\bar{b}} = \frac{2 c_V}{1 + \left(\frac{c_V}{c_A} \right)^2}$$

the c_V/c_A COUPLING INCLUDES THE
CHANGE IN 6 CHARGE

$$c_V = I_w^{(3)} - 2Q \sin^2 \theta_w$$

$$c_A = I_w^{(7)}$$

Good!
AGAIN, YOU
COULD'VE
COMPARED WITH
THE PREDICTION
FOR THE
VARIOUS CASES

III FORWARD-BACKWARD ASYMMETRY

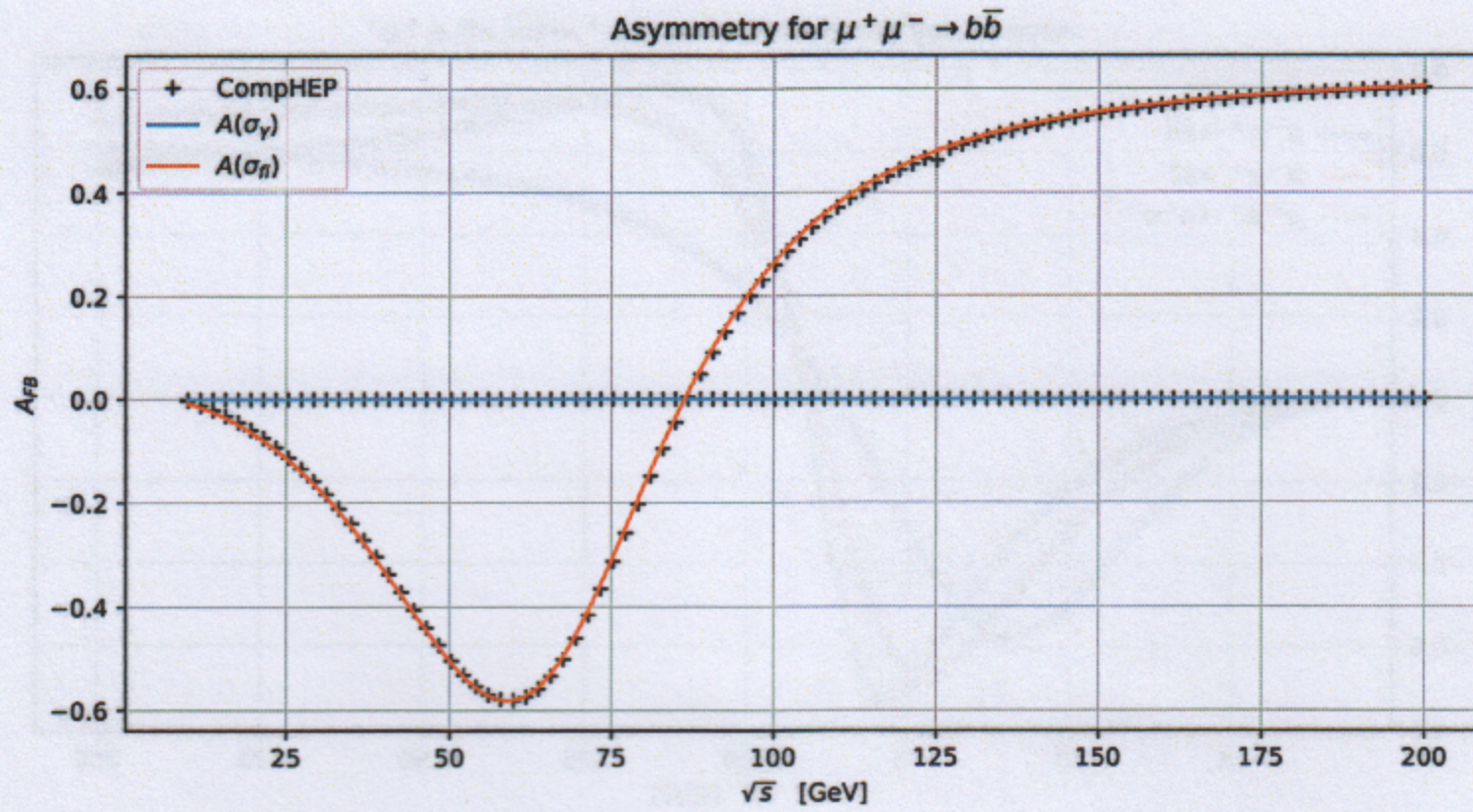


FIG. 4: The total asymmetry for $\mu^+\mu^- \rightarrow b\bar{b}$ and the asymmetry for the pure QED process. This is zero, as expected. Data generated in CompHEP are marked with black plus(+) signs

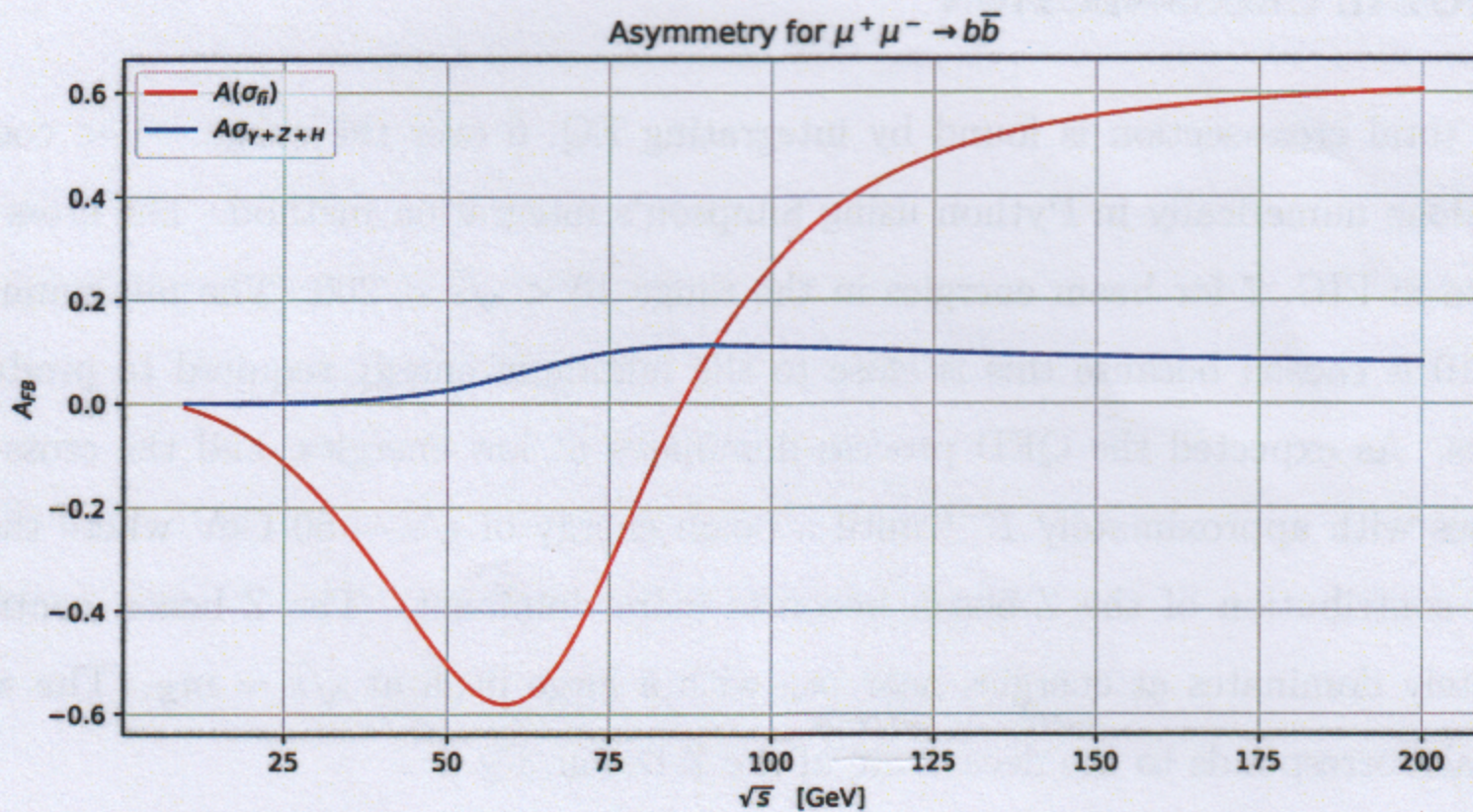


FIG. 5: The asymmetry factor without the contribution from the interference term.

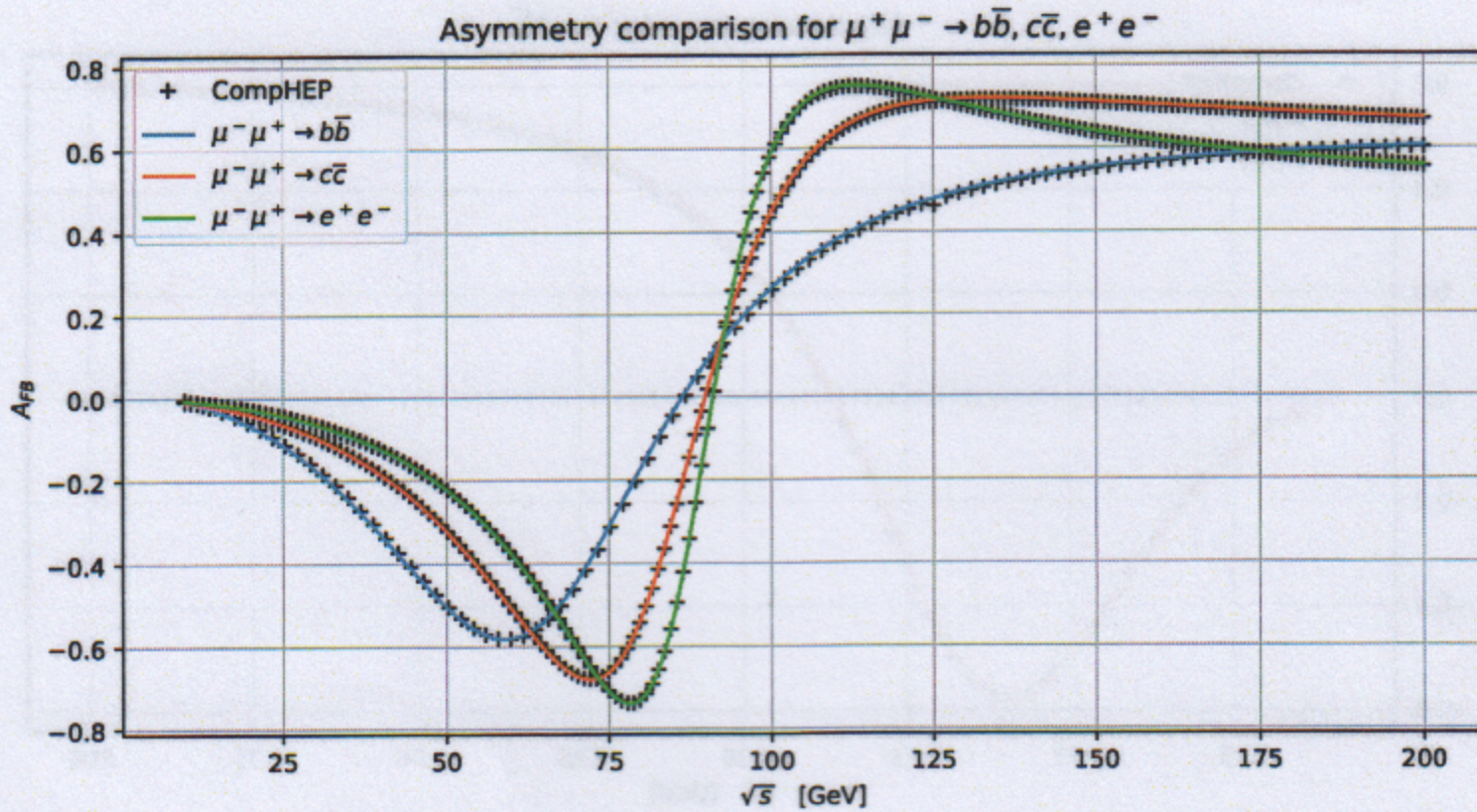


FIG. 6: Comparison of the forward-backward asymmetry for final states with $b\bar{b}$, $c\bar{c}$ and e^+e^- . Data generated in CompHEP are marked with black plus(+) signs.

IV. TOTAL CROSS-SECTION

The total cross-section is found by integrating EQ. 6 over the range $-1 < \cos\theta < 1$, this is done numerically in Python using Simpson's integration method. The cross-section is shown in FIG. 7 for beam energies in the range $10 < \sqrt{s} < 200$. The minimum energy $\sqrt{s} = 10$ is chosen because this is close to the minimum energy required to produce two b -quarks. As expected the QED process dominates at low energies, and the cross-section decreases with approximately E^{-2} until a beam energy of $\sqrt{s} \sim 50$ GeV where the cross-section contribution of the Z-boson becomes more dominant. The Z-boson contribution completely dominates at energies near m_Z with a large peak at $\sqrt{s} = m_Z$. The width of this peak corresponds to the decay rate of the Z-boson, Γ_Z .

The total cross-section for the individual contributions to the processes are shown in FIG. 8 together with data gathered in CompHEP. For both the Z and H contribution (FIG.8a and 8b) we can see a spike in the cross-section at $\sqrt{s} = m_Z$ and $\sqrt{s} = m_H$ respectively.

IV TOTAL CROSS-SECTION

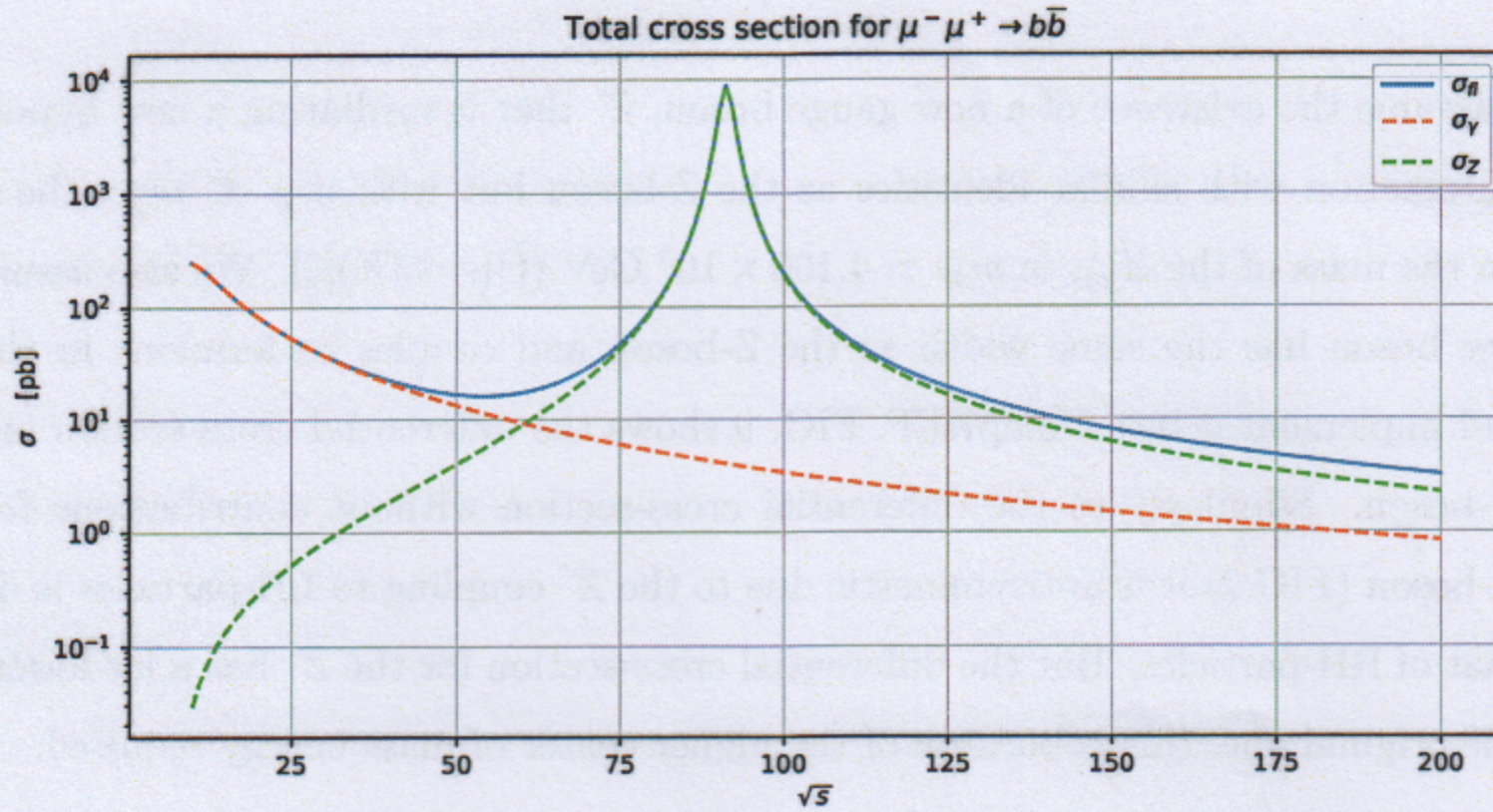


FIG. 7: Total cross-section for $\mu^+ \mu^- \rightarrow b\bar{b}$ compared with the contributions from the pure QED process and the pure NC-WI process.

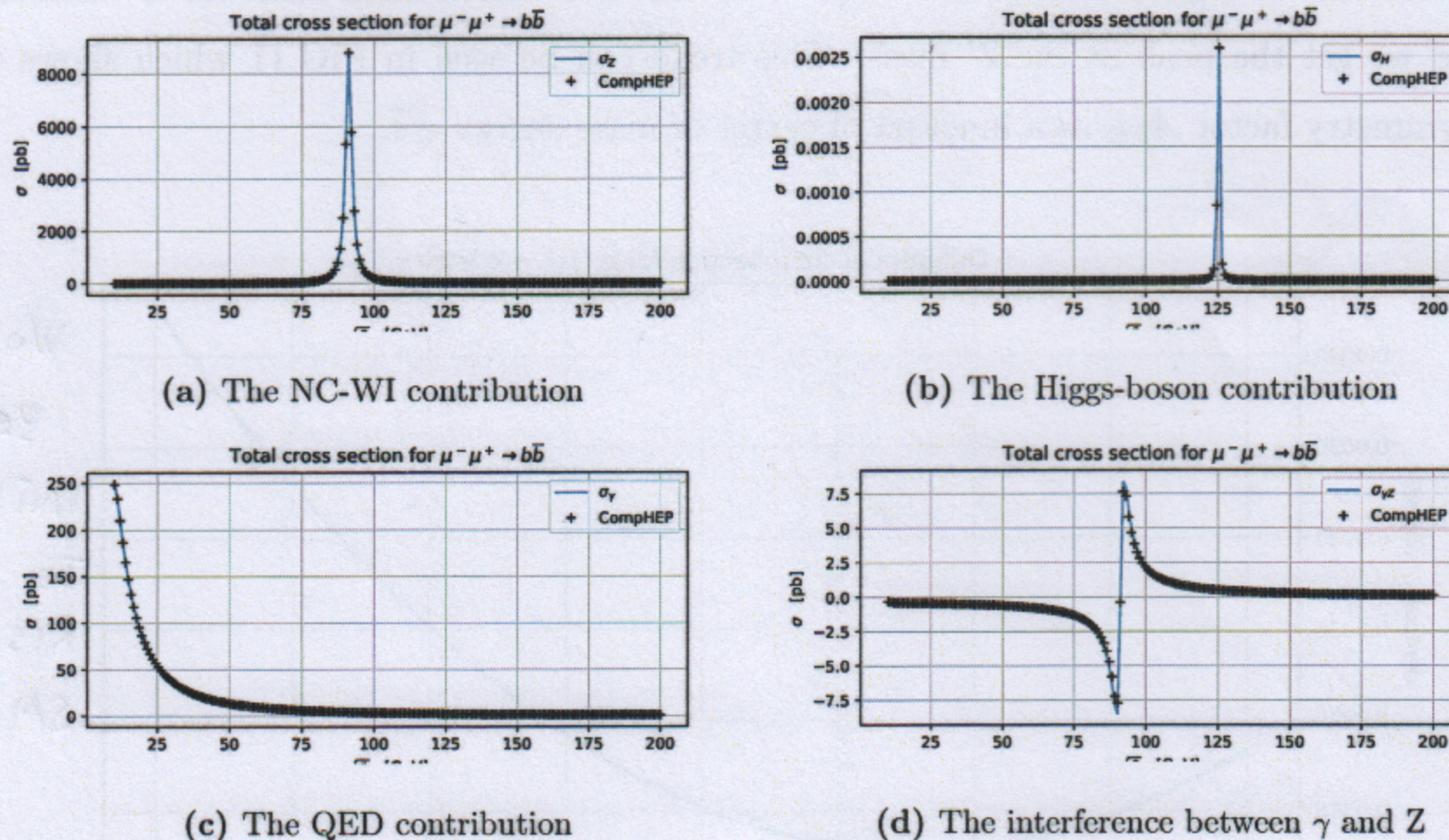


FIG. 8: Individual contributions to the total cross-section. The black plus(+) sign represents data generated in CompHEP

V. NEW PHYSICS

We assume the existence of a new gauge boson, Z' that is mediating a new hypothetical weak interaction with similar identities as the Z-boson but with $m_Z \ll m_{Z'}$, the current limit on the mass of the Z'_{SM} is $m_{Z'} > 4.100 \times 10^3$ GeV (CL=95%)[2]. We also assume that this new boson has the same width as the Z-boson and couples to fermions in the same way, and implement it into CompHEP. FIG. 9 shows the differential cross-section including this Z' -boson. Similarly to the differential cross-section without contributions from the new Z' -boson (FIG.2) it is antisymmetric due to the Z' coupling to LH-particles is different than that of RH-particles. But the differential cross-section for the Z' has a lot lower values than the original one, this is because of the higher center of mass energy required.

The total cross-section in FIG.10 shows clear resonances at both $\sqrt{s} = m_Z$ and $\sqrt{s} = m_{Z'}$ as we would expect. The cross-section is dominated by the QED process at low energies and Z-around the Z-mass just as it was in FIG. 7, but as the energy increases further the interference of the Z' takes effect. At $\sqrt{s} \sim 3.4$ TeV the contribution from the Z' dominates and we get the peak at the Z' mass. This trend can be seen in FIG.11 which shows the asymmetry factor A_{FB} as a function of center of mass energy \sqrt{s} .

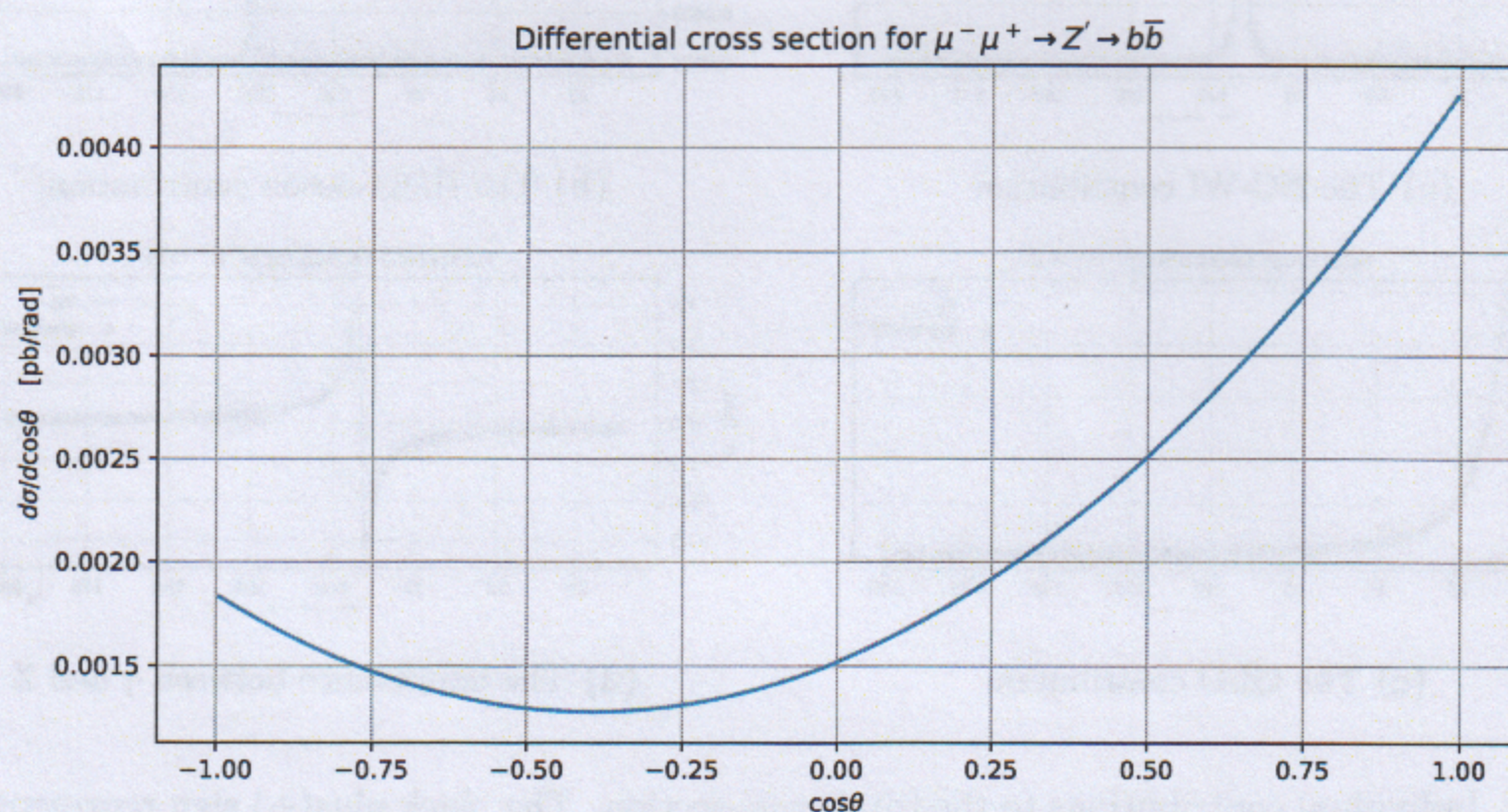


FIG. 9: CompHEP generated differential cross-section at $\sqrt{s} = 1.5$ TeV including contributions from Z' with $m_{Z'} = 4.5$ TeV

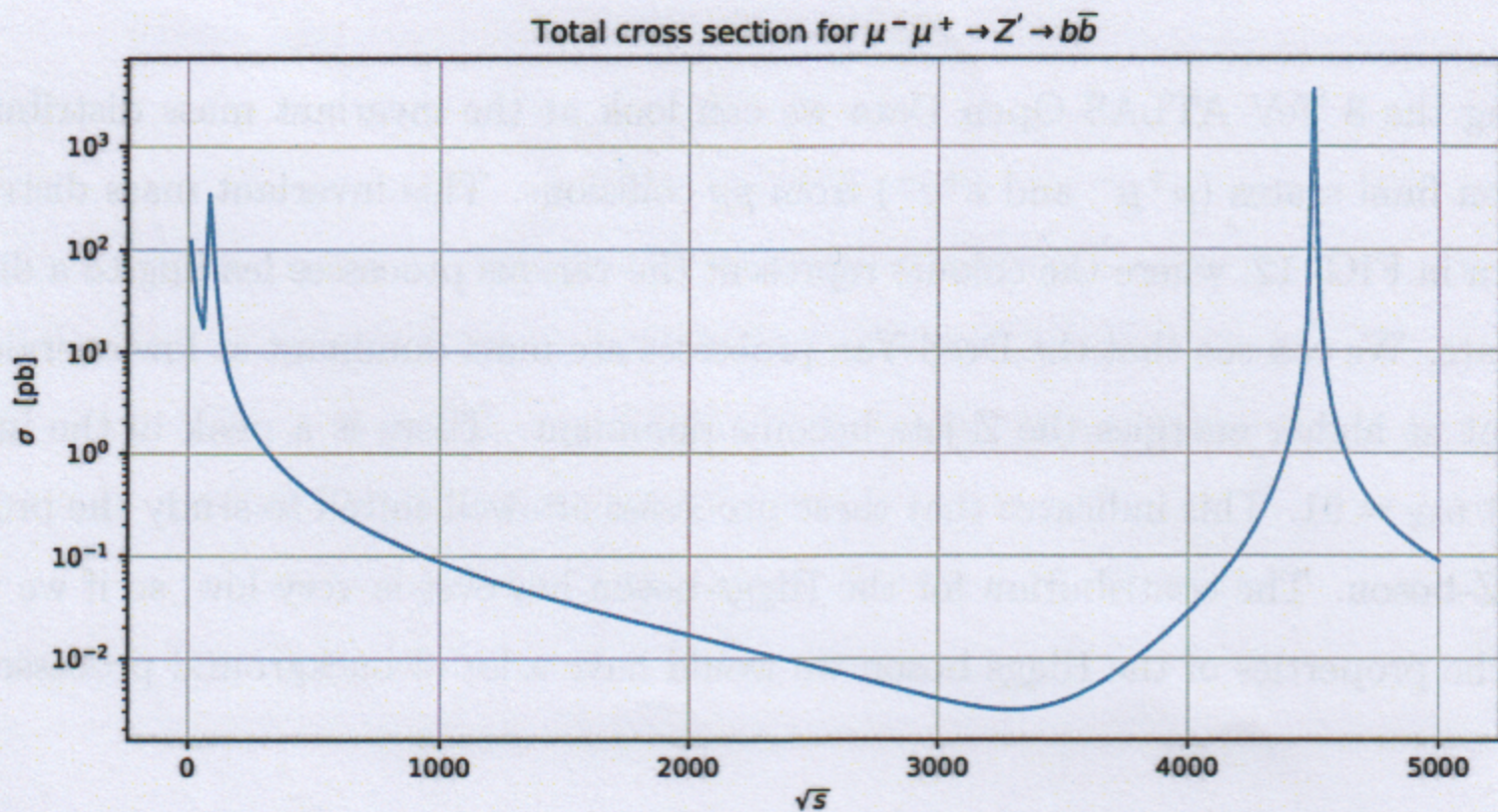


FIG. 10: CompHEP generated total cross-section including contributions from a Z' with $m_{Z'} = 4.5\text{TeV}$

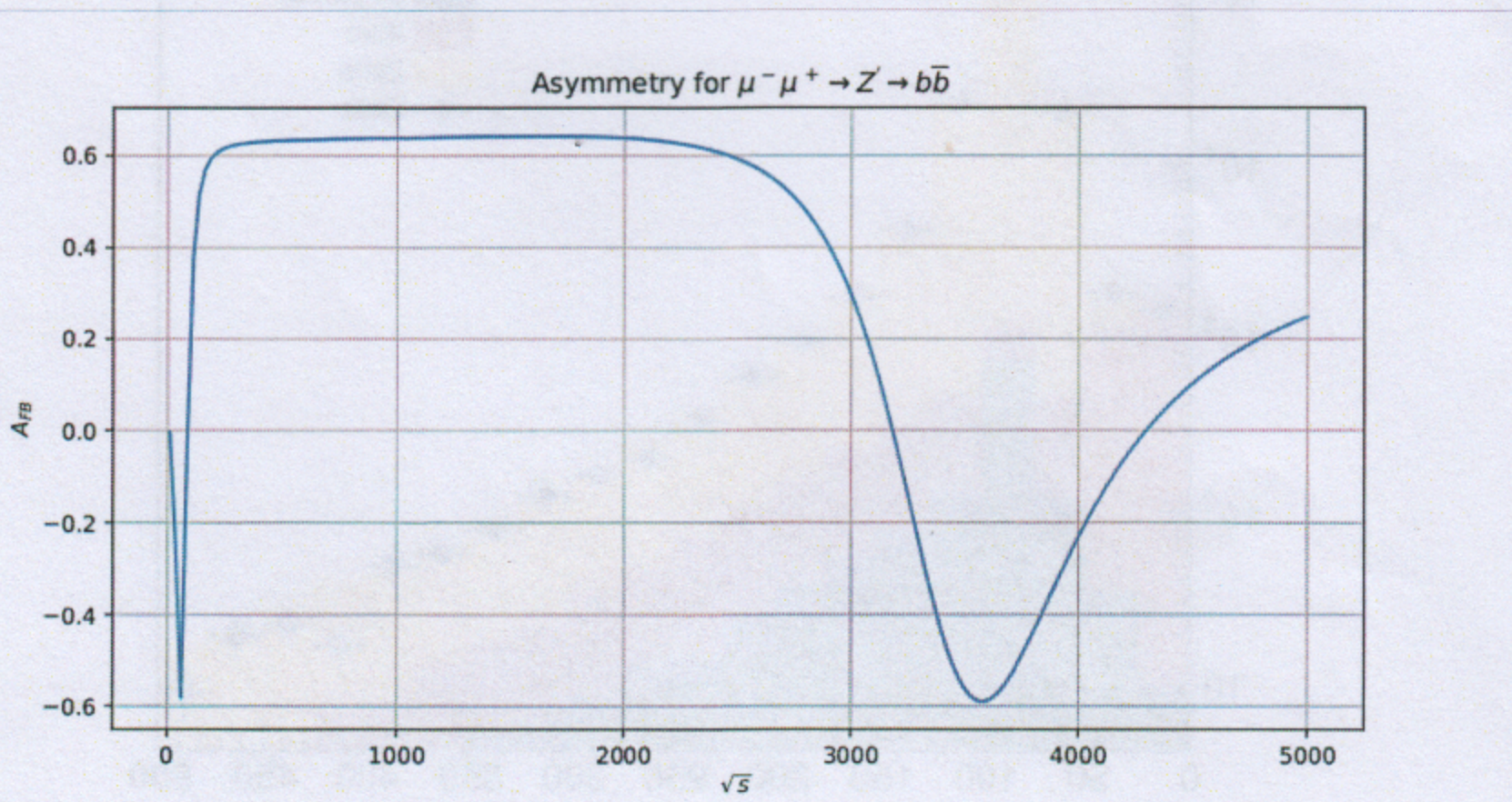


FIG. 11: CompHEP generated forward-backward asymmetry including contributions from a Z' with $m_{Z'} = 4.5\text{TeV}$

AGAIN; WOULD'VE BEEN GOOD WITH A COMPARISON
WITH SM (NO Z'). THIS IS A WAY TO DISCOVER
NEW PARTICLES EVEN IF THE ENERGY IS NOT
LARGE ENOUGH TO PRODUCE THEM DIRECTLY

VI. ATLAS DATA ANALYSIS

Using the 8 TeV ATLAS Open Data we can look at the invariant mass distribution of di-lepton final states ($\mu^+\mu^-$ and e^+e^-) from pp collisions. This invariant mass distribution is shown in FIG. 12, where the colours represent the various processes leading to a di-lepton final state. We can see that the Drell-Yan processes are most dominant at low energies ~ 25 GeV but at higher energies the Z-jets become dominant. There is a peak in the invariant mass at $m_Z = 91$. This indicates that these processes are well suited to study the properties of the Z-boson. The contribution for the Higgs-boson however is very low, so if we were to study the properties of the Higgs boson we would have a lot of background processes.

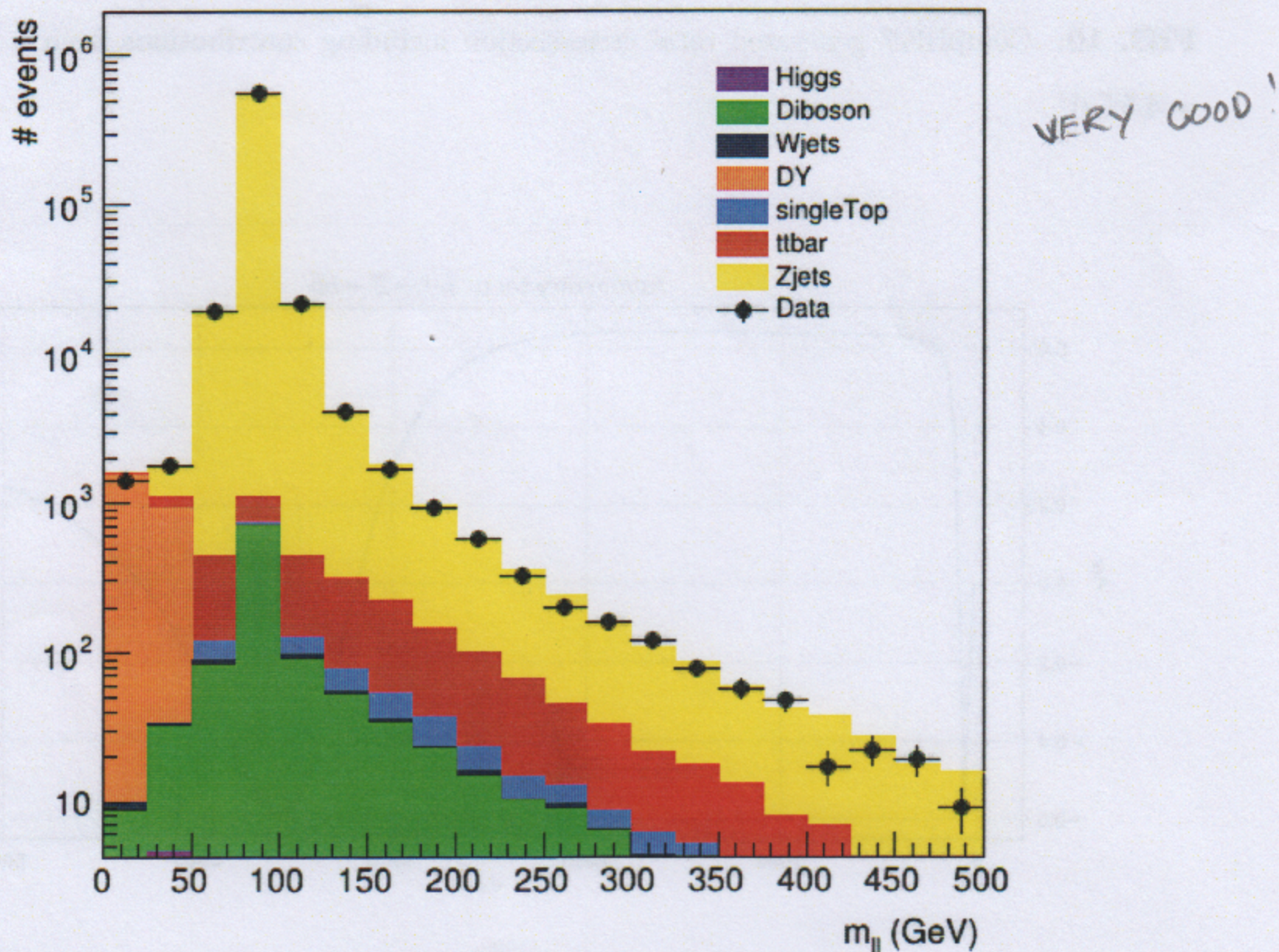


FIG. 12: Invariant mass distribution of di-leptons in 8 TeV ATLAS Open Data

VII. APPENDIX

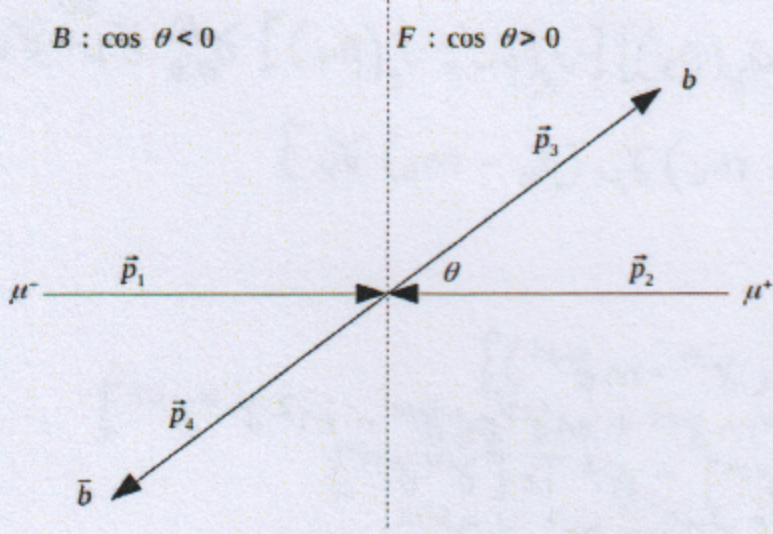


TABLE I: The fundamental fermions and their couplings to the Z assuming $\sin^2 \theta_W = 0.23146$ [1]

Fermion	c_V	c_A	Q_f
ν_e, ν_μ, ν_τ	+0.5	+0.5	0
e^-, μ^-, τ^-	-0.04	-0.5	-1
u, c, t	+0.19	+0.5	$+\frac{2}{3}$
d, s, b	-0.35	-0.5	$-\frac{1}{3}$

FIG. 13: The momentum vectors in the center of mass frame

- [1] M. Thomson, *Modern Particle Physics*, Cambridge University Press, 2019
- [2] M. Tanabashi *et.al* (Particle Data Group), Phys.Rev.D **98**, 030001 (2018)
- [3] S. Braibant, G.Giacomelli, M. Spurio *Particles and Fundamental Interactions* Springer, 2009
- [4] <https://github.com/Etienne357/FYS5555>
- [5] <https://twiki.cern.ch/twiki/bin/view/Main/CompHep>